2. SIMULATION OF 2-D VELOCITY DISTRIBUTION IN A STRATIFIED INCOMPRESSIBLE REACTIVE FLOW WITH BUOYANT TERM

Applications where the density remains uniform across the domain are assumed incompressible and, as stated before, stratified flows under the scope of this thesis may be treated as incompressible. In such flows, the Navier-Stokes equations may be generally expressed in two different formulations, based on the dependent variables used. If expressed in terms of velocity and pressure, it is termed primitive variables formulation. If incorporating definitions of vorticity and stream function, it is named as the vorticity-stream function formulation.

The use of vorticity-stream function formulation in 2-D problems is possible, since the stream function exists for planar or axisymmetric flows only (HOFFMAN; CHANG, 2000). It must be noted, however, that for three-dimensional purposes, it is possible to extend the vorticity-stream function approach by the use of the so-called vector potential–that is not, however, covered here.

In the preceding section, the species concentration equation assuming an uncoupled flow velocity profile was solved. Now, with the aim of coupling the velocity profile, in order to solve the system encompassed by Equations 2 to 4, a model based on stream-function and vorticity is developed. It is to emphasize that this coupling allows the building of a nonlinear model with respect to the flow dynamics, because velocities will be approached in every node of the discretized domain.

The Boussinesq hypothesis is now employed in a novel formulation, in order to represent the density variation of a stratified flow due to gas solute concentration differences, which is also a nonlinear feature of the model, as it will be following shown.

2.1 Literature Review

Incompressible flows, with or without chemical reactions, have been often approached by vorticity-stream function formulations and the advantages of its use for two-dimensional computations are well known (TEZDUYAR et al., 1990). For instance, in 2-D simulations, the vorticity-stream function equations reduce to a set of scalar equations for only two unknowns and the incompressibility constraint is automatically satisfied by the flow field (GLAISNER; TEZDUYAR, 1987). Also, the vorticity field is obtained directly rather than by differentiation of the velocity field (TEZDUYAR et al., 1988).

However, there are difficulties in this formulation associated with the convection term in the vorticity and species transport equations and the lack of boundary conditions for the vorticity at no slip boundaries. The determination of vorticity in such boundaries can be derived from the Poisson Equation for the stream function. Methods of doing this with FEM are addressed, with more or less details, by Taylor and Hood (1973) and by Glowinski and Pironneau (1977) for Dirichlet BCs, by Campion-Renson and Crochet (1978) by solving the equations simultaneously without the use of wall vorticity formulae, by Bristeau et al. (1987), for prescribed and Neumann BC in a semi-explicit numerical scheme, by Dhatt et al. (1981) and by Peeters et al. (1987), who developed similar methods of imposing BC on the stream function equation through variational formulations. Glaisner and Tezduyar (1987) summarized these methods, suggesting to consider the wall vorticity as unknowns in the discrete Poisson Equation in unsteady transports, consideration that was later used on the

investigation of proper downstream BC for the vorticity-stream formulation of 2-D incompressible fluids (TEZDUYAR; LIOU, 1991).

Adequate uncoupling of stream function and vorticity, following the main lines of the Glowinski-Pironneau method for the unsteady transport equations, may be easily programmed, because there is no iteration required to recover the boundary values for the vorticity (JIAN-GUO, 2000). Also, it might be a feature to overcome the difficulty arising from the lack of BC for the vorticity on the no-slip boundaries (GHADI et al., 2008 &2013).

It must be highlighted also that considering the right downstream BC for environmental cycle driven flows is a problem that must be addressed properly. This matter was handled in Section 1, concerning the determination of the concentration species, where a comprehensive literature review regarding time dependent BCs was presented. A new form of boundary condition, termed MDBC, was developed and this concept may be applied to the vorticity transport equation.

Also, considering vorticity BCs, classical papers dealing with 3-D formulation may be cited as the works of Aziz and Hellums (1967), Hirasaki (1967), Aregbesola and Burley (1977), Wong and Reizes (1984) and Tutty (1986). They are centered on 3-D problems and do not apply explicitly to the present scope, but do provide some interesting contribution by defining BCs for the vorticity transport at solid surfaces which may be of use.

2.2 **Mathematical Formulation**

2.2.1 Weak formulation of the transport equations

The formulation is developed under the assumption of subcritical flow along all the domain, comprised by the reservoir basin, and gravity is the driven force to impart an open reservoir flow, rather than pressure gradient.

Equations 2 and 3 constitute the momentum transfer equations in the vorticity-stream function formulation. The buoyant term in Equation 2 is introduced according to the Boussinesq hypothesis. It states that the density variation is only important in the gravity force term, ρg, and can be neglected in the rest of the equation.

So, considering primitive formulation, we have for an incompressible flow:

$$\rho_o\left(\frac{\partial \vec{u}}{\partial t} + (\vec{u}\cdot\nabla)\vec{u}\right) = -\nabla p + \mu\nabla^2\vec{u} + \rho\vec{g} \tag{55}$$

where the temperature dependent density, ρ, is replaced by a constant density, ρ_o, except in the body force term. This term can be rewritten as $(\rho_o+\Delta\rho)g$, where $\Delta\rho$ represents the density variation with respect to the reference density, or $\rho - \rho_o$, which yields:

$$\rho_o\left(\frac{\partial \vec{u}}{\partial t} + (\vec{u}\cdot\nabla)\vec{u}\right) = -\nabla p + \mu\nabla^2\vec{u} + (\rho_o + \Delta\rho)\vec{g} \tag{56}$$

By taking the curl of the above equation, or:

$$\nabla\times\left(\frac{\partial \vec{u}}{\partial t} + (\vec{u}\cdot\nabla)\vec{u}\right) = \nabla\times\left(\frac{-\nabla p}{\rho_o} + \nu_o\nabla^2\vec{u} + \vec{g}\,\frac{\rho}{\rho_o}\right) \tag{57}$$

where $\nu_o = \frac{\mu}{\rho_o}$, we obtain the vorticity-stream function form (AZIZ; HELLUMS, 1967), as presented by Equation 2, remembering that $\rho^* = \rho / \rho_o$ and **rot** $\psi = \vec{u}$. Further insight may be found in Rehm and Baum (1978), Rehm et al. (1982) and Kawala and Odda (2013).

In order to reach an approximation through FEM, the weighted residual statements for a bi-dimensional form of Equations 2 and 3 read, respectively:

$$\int_\Omega \left(\frac{\partial \omega}{\partial t} + \frac{\partial \psi}{\partial y}\frac{\partial \omega}{\partial x} - \frac{\partial \psi}{\partial x}\frac{\partial \omega}{\partial y} - \nu_o \left(\frac{\partial^2 \omega}{\partial x} + \frac{\partial^2 \omega}{\partial y} \right) + \frac{\partial \rho^*}{\partial x} g_y \right) w d\Omega = 0 \tag{58}$$

$$\int_\Omega \left(\frac{\partial^2 \psi}{\partial x} + \frac{\partial^2 \psi}{\partial y} + \omega \right) w d\Omega = 0 \tag{59}$$

where w is an arbitrary weight function and Ω is the control volume encompassing the domain.

By applying conveniently the divergence theorem to the above equations, the following weak forms are obtained:

$$\int_\Omega \left(w\frac{\partial \omega}{\partial t} + w\frac{\partial \psi}{\partial y}.\frac{\partial \omega}{\partial x} - w\frac{\partial \psi}{\partial x}.\frac{\partial \omega}{\partial y} + \nu_o \left(\frac{\partial w}{\partial x}.\frac{\partial \omega}{\partial x} + \frac{\partial w}{\partial y}.\frac{\partial \omega}{\partial y} \right) + w\frac{\partial \rho^*}{\partial x} g_y \right) d\Omega = \int_\Gamma w \nu_o \left(n_x . \frac{\partial \omega}{\partial x} + n_y . \frac{\partial \omega}{\partial y} \right) d\Gamma \tag{60}$$

$$\int_\Omega \left(\frac{\partial w}{\partial x}\frac{\partial \psi}{\partial x} + \frac{\partial w}{\partial y}\frac{\partial \psi}{\partial y} \right) d\Omega - \int_\Gamma w \left(n_x . \frac{\partial \psi}{\partial x} + n_y . \frac{\partial \psi}{\partial y} \right) d\Gamma = \int_\Omega w \omega d\Omega \tag{61}$$

where, $n_x = \vec{n} \cdot \vec{e}_x$, $n_y = \vec{n} \cdot \vec{e}_y$ and $\Gamma = \Gamma_{in} \cup \Gamma_1 \cup \Gamma_2 \cup \Gamma_3 \cup \Gamma_{out}$ are defined in Figure 14, depicting the shape chosen to represent an hypothetical reservoir basin. Figure 14 also presents BCs defined for these boundaries.

Figure 14 – Domain surfaces and boundary conditions

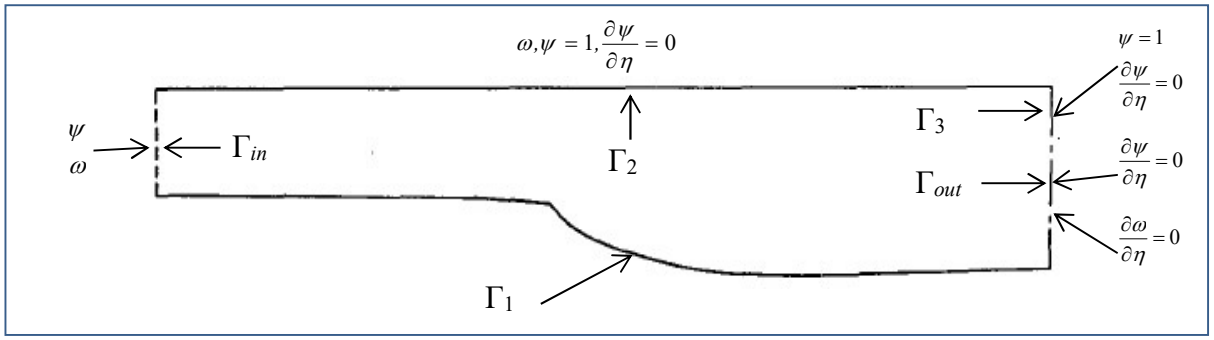

Source: Adapted from PEETERS et al. (1987).

2.2.2 Formulation of boundary conditions

The upper surface (Γ_2) is open to the atmosphere, so, the stream function at the inlet (Γ_{in}) is designed as a predefined semi parabolic velocity profile, typical of such entries. Adopted inlet parameters corresponding to Figure 14 are summarized in Table 4.

In order to represent cyclic variations of environmental phenomena, assuming that u is time periodic and has a Fourier representation, the velocity profile may be multiplied by (1+ $cos\ m\pi t$). By doing so, this term will also be present in the stream function and vorticity expressions.

Table 4 – Prescribed inlet parameters.

Parameter	Profile
Horizontal Velocity (u_x)	$3y - 1.5y^2$
Stream Function (ψ)	$1.5y^2 - y^3/2$
Vorticity (ω)	$3y - 3$

Once the boundary stream function for all surfaces, but Γ_{out}, is imposed, the weighting function at those boundaries vanishes. For the outlet, Neumann homogeneous condition is suggested for the stream function (PEETERS et al., 1987). This implies in zero tangential velocity, what may be too restrictive at a first glimpse. But the assumption that the velocity vector is not inclined may be well adjusted to the problem in sight. Thus, the following form of Equation 61 for the Poisson Equation applies:

$$\int_{\Omega}\left(\frac{\partial w}{\partial x}\frac{\partial \psi}{\partial x}+\frac{\partial w}{\partial y}\frac{\partial \psi}{\partial y}\right)d\Omega=\int_{\Omega} w\omega d\Omega \tag{62}$$

Determination of the vorticity at no-slip boundaries poses serious difficulties for the formulation, as already mentioned. However, values may be reached through the solution of the above equation after the stream function is computed for all the domain, as suggested by Glaisner and Tezduyar (1987) and others. This procedure is implemented computationally, as described further in the text.

For the outlet vorticity, one of the three types presented by Equations 5 to 6 may be used, applied to vorticity transport. But in case of environmental time dependent inlet conditions, presetting outlet conditions may lead to inconsistent solutions. It must be also remarked that setting the vorticity normal derivative to zero is quite reasonable for advection dominated flows (TEZDUYAR; LIOU, 1991), but it does not hold if the gradients are not zero or not constant. The study in sight is particularly interested in situations that arise from time or cyclic variations of upstream conditions and may imply in variable or non-zero gradients downstream.

Thus, another way must be thought of. By chance, it may be assumed that $\vec{n}=\vec{e}_x$ at the outlet and, therefore, the r.h.s. of Equation 60 becomes:

$$\int_{\Gamma_{out}} w\nu_o\left(\frac{\partial \omega}{\partial x}\right)d\Gamma_{out} \tag{63}$$

Adopting proposition of several authors to take as downstream BC the inviscid momentum equation (Equation 18), we obtain by modifying Equation 56:

$$\frac{\partial \vec{u}}{\partial t}+(\vec{u}\cdot\nabla)\vec{u}=\frac{-\nabla p}{\rho_o}+\vec{g}\rho^{*} \tag{64}$$

By taking the curl of the above equation, again remembering that vorticity (ω) is defined as:

$$\nabla \times \vec{u} = \omega \tag{65}$$

a vorticity form is obtained and a BC for the outlet based on the vorticity time derivative which evaluates the vorticity flux is reached.

In the case of a two-dimensional flow (AZIZ; HELLUMS, 1967 & GLAISNER; TEZDUYAR, 1987) it reads:

$$\frac{\partial \omega}{\partial t} + (\vec{u} \cdot \nabla)\omega = -\frac{\partial \rho^*}{\partial x} g_y \tag{66}$$

thus: $$\vec{u}.\nabla \omega = -\left(\frac{\partial \omega}{\partial t} + \frac{\partial \rho^*}{\partial x} g_y \right) \tag{67}$$

Next, by assuming that at the boundary Γ_{out}, $\vec{u} = \vec{n}\overline{U}$, where $\overline{U} = \sqrt{\overline{u}_x^2 + \overline{u}_y^2}$ Equation 67 implies in:

$$\vec{n}.\nabla \omega = -\frac{1}{\overline{U}} \left(\frac{\partial \omega}{\partial t} + \frac{\partial \rho^*}{\partial x} g_y \right) \tag{68}$$

which is a BC for the vorticity transport equation similar to the MDBC defined for the species conservation equation in the previous section and also found in Oliveira Filho et al. (2017).

Recalling that $\vec{n} = \vec{e}_x$ for the outlet, Equation 63 may be expressed by:

$$\int_{\Gamma_{out}} -w \frac{\nu_o}{\overline{U}} \left(\frac{\partial \omega}{\partial t} + \frac{\partial \rho^*}{\partial x} g_y \right) d\Gamma_{out} \tag{69}$$

Then, the weak formulation of the vorticity transport equation comprises Equation 60, with its r.h.s., given by Equation 69, and the Poisson Equation for the stream function, given by Equation 62.

It may also be added that, if the stream function is assumed in the form of the downstream BC, Equation 66 would be expressed by:

$$\frac{\partial \omega}{\partial t} + \nabla \times \psi \cdot \nabla \omega = \frac{\partial \rho^*}{\partial x} g_y \tag{70}$$

implying in:

$$\frac{\partial \psi}{\partial y}\frac{\partial \omega}{\partial x} - \frac{\partial \psi}{\partial x}\frac{\partial \omega}{\partial y} = -\left(\frac{\partial \omega}{\partial t} + \frac{\partial \rho^*}{\partial x} g_y \right) \tag{71}$$

and leading to:

$$\vec{n}.\nabla \omega = \frac{1}{\overline{U}} \left(\frac{\partial \psi}{\partial y}\frac{\partial \omega}{\partial x} - \frac{\partial \psi}{\partial x}\frac{\partial \omega}{\partial y} \right) \tag{72}$$

With this approach, it is possible to reach from Equation 60:

$$\int_{\Omega} \left(w\frac{\partial \omega}{\partial t} + w\frac{\partial \psi}{\partial y}.\frac{\partial \omega}{\partial x} - w\frac{\partial \psi}{\partial x}.\frac{\partial \omega}{\partial y} + \nu_o \left(\frac{\partial w}{\partial x}.\frac{\partial \omega}{\partial x} + \frac{\partial w}{\partial y}.\frac{\partial \omega}{\partial y} \right) + w\frac{\partial \rho^*}{\partial x} g_y \right) d\Omega =$$

$$= \int_{\Gamma} w \frac{\nu_o}{\overline{U}} \left(\frac{\partial \psi}{\partial y} \frac{\partial \omega}{\partial x} - \frac{\partial \psi}{\partial x} \frac{\partial \omega}{\partial y} \right) d\Gamma \tag{73}$$

Equation 73 points at a new form of determining nonhomogeneous Neumann BCs, but it applies only to specific cases where tangential and normal derivatives of the stream function are not zero. It is easy to see that when these derivatives are zero, as in the present case, it would imply in total irrelevance of the vorticity BC what seems to be inconsistent with the adopted model.

However, Equation 73 also provides another way of avoiding arbitrarily preset data for variable input and, probably, it could be applied to cases where the velocity vector at the exit is inclined and also in the case of permeable upper and lower surfaces. Obviously, Equation 73 does not provide a MDBC type boundary condition and it would not benefit from the procedures already implemented in the preceding section for species concentration simulations. So, this is left as a suggestion for future works.

In order to provide a comprehensive analysis by comparing simulations outcomes, use of outlet EBC and NBC is also intended. Although considered the less realistic ones, it is possible to adopt EBCs summarized below at the edge of the exiting flow.

Table 5 – Imposed outlet parameters.

Parameter	Profile
Horizontal Velocity (u)	$\overline{U}$
Stream Function (ψ)	Y
Vorticity (ω)	0.0

Where Y represents corrected coordinate values of the dam opening, supposedly zero at its bottom and unitary at its upper end, implying in a linear profile for the stream function, and $\overline{U} = \frac{2}{3} U_{max}$, in correspondence to the entry profile.

For EBC and NBC at the outlet, vorticity transport formulation reduces to:

$$\int_{\Omega} \left(w \frac{\partial \omega}{\partial t} + w \frac{\partial \psi}{\partial y} . \frac{\partial \omega}{\partial x} - w \frac{\partial \psi}{\partial x} . \frac{\partial \omega}{\partial y} + \nu_o \left(\frac{\partial w}{\partial x} . \frac{\partial \omega}{\partial x} + \frac{\partial w}{\partial y} . \frac{\partial \omega}{\partial y} \right) + w \frac{\partial \rho^*}{\partial x} g_y \right) d\Omega = 0 \tag{74}$$

while Equation 62 also applies to these cases.

It is also of practical interest to analyze cases of wind blowing tangentially to the reservoir water level surface. Generalization of a parabolic velocity profile for the water flow, keeping the same shape as adopted inlet conditions, reads:

$$u_x = a_2 y^2 + a_1 y \tag{75}$$

The derivative of this profile coupled to the definition of Newtonian fluids, which fits to water in reservoirs, gives the stress profile of the fluid, or:

$$\frac{\partial u_x}{\partial y} = 2a_2 y + a_1 = -\frac{\tau_y}{\mu} \tag{76}$$

where, from the definition of vorticity (Equation 3), it may be concluded that:

$$\frac{\tau_y}{\mu} = \omega \tag{77}$$

Equation 77 points at a way of assuming a tangential wind blowing at Γ_2. If zero vorticity is imposed at that surface, as depicted in Figure 14, it means that the deformation stress is minimum, what means no wind. By the contrary, if the vorticity is not zero, it implies in the existence of a given tangential stress, due to wind blowing.

Thus, the entry profile is modified, because, at the surface (y = 1):

$$2a_2 + a_1 = -\frac{\tau_s}{\mu} = -\omega_s \tag{78}$$

and so, it is shown that profile coefficients may be defined in terms of the superficial vorticity and vice-versa. In consequence, several particular solutions may be generated due to variable values for entry velocity profile or surface vorticity.

2.2.3 Introduction of the buoyant term

In the flow under consideration, where water density is a weak function of the temperature (Equation 1) that comprises itself an uncoupled field, it is reasonable to assume that the flow density is influenced by mixed gases concentration, or $\rho = \rho(C)$. It is also expected that mixing of gases implies in the decreasing of the water standard density values. Thus, assuming it in linear form, one has as an initial condition:

$$\rho = \rho_o - bC \tag{79}$$

where b is a parameter that fits the gases concentration to the water density reduction term

This linear dependence hypothesis can well represent the water density–depth stratification scheme for reservoirs proposed by Boegman (2009). In the cases of not uniform mixing of the gases, the density assumes local values according to local gases concentration values, as it is expected.

If Equation 79 is divided by ρ_o, one has:

$$\rho^* = 1 - \frac{b}{\rho_o} C \tag{80}$$

Then, from Equation 80, is possible to attain a more useful form for the buoyant term, which is:

$$\frac{\partial \rho^*}{\partial x} g_y = -\frac{b}{\rho_o} \frac{\partial C}{\partial x} g_y \tag{81}$$

Following, Equation 60 with its r.h.s given by Equation 69 merges handily in:

$$\int_{\Omega} \left(w\frac{\partial \omega}{\partial t} + w\frac{\partial \psi}{\partial y}.\frac{\partial \omega}{\partial x} - w\frac{\partial \psi}{\partial x}.\frac{\partial \omega}{\partial y} + \nu_o \left(\frac{\partial w}{\partial x}.\frac{\partial \omega}{\partial x} + \frac{\partial w}{\partial y}.\frac{\partial \omega}{\partial y} \right) - w\frac{b}{\rho_o}\frac{\partial C}{\partial x} g_y \right) d\Omega =$$

$$= \int_{\Gamma_{out}} w \frac{\nu_o}{\overline{U}} \left(\frac{b}{\rho_o}\frac{\partial C}{\partial x} g_y - \frac{\partial \omega}{\partial t} \right) d\Gamma_{out} \tag{82}$$

As previously stated, for outlet prescribed BCs, as well as for NBC, the r.h.s of Equation 82 does not apply and is not taken into account in the formulation.

2.3 **Numerical Procedure**

2.3.1 Variables approximation and discretization of the equations

In FEM, the variables are approximated by:

$$\omega_{appr}(x_i,t)=\sum_{j=1}^{NN}\omega_j(t)S_j(x_i) \tag{83}$$

$$\psi_{appr}(x_i,t)=\sum_{j=1}^{NN}\psi_j(t)S_j(x_i) \tag{84}$$

Inserting these approximations and the one given by Equation 22 in the weak form of the vorticity transport equation given by Equation 82:

$$\sum_{j=1}^{NN}\left\{\left(\int_\Omega S_iS_j d\Omega+\frac{\nu_o}{\overline{U}}\int_{\Gamma_{out}}S_iS_j d\Gamma_{out}\right)\frac{d\omega_j}{dt}+\int_\Omega\left[S_i\left(\frac{\partial\psi^e}{\partial y}\frac{\partial S_j}{\partial x}-\frac{\partial\psi^e}{\partial x}\frac{\partial S_j}{\partial y}\right)+\nu_o\left(\frac{\partial S_i}{\partial x}\frac{\partial S_j}{\partial x}+\right.\right.\right.$$

$$\left.\left.\left.+\frac{\partial S_i}{\partial y}\frac{\partial S_j}{\partial y}\right)\right]d\Omega\omega_j\right\}=\sum_{j=1}^{NN}\left\{\frac{b}{\rho_o}\left(\int_\Omega S_i\frac{\partial S_j}{\partial x}d\Omega+\frac{\nu_o}{\overline{U}}\int_{\Gamma_{out}}S_i\frac{\partial S_j}{\partial x}d\Gamma_{out}\right)g_{x_2}C_j\right\} \tag{85}$$

where ψ^e is the stream function inside each element (KONZEN et al., 2007), approximated by:

$$\psi^e_{appr}=\sum_{j=1}^{NEN}\psi^e_j(t)S_j(x_i) \tag{86}$$

and NEN refers to number of nodes in each element, three or four, according to the mesh generation option, implying in:

$$\frac{\partial\psi^e}{\partial x}=\sum_{j=1}^{NEN}\frac{\partial S_j}{\partial x}\psi^e_j \quad \text{and} \quad \frac{\partial\psi^e}{\partial y}=\sum_{j=1}^{NEN}\frac{\partial S_j}{\partial y}\psi^e_j \tag{87}$$

For prescribed or natural type outlet BC, one has:

$$\sum_{j=1}^{NN}\left\{\left(\int_\Omega S_iS_j d\Omega\right)\frac{d\omega_j}{dt}+\int_\Omega\left[S_i\left(\frac{\partial\psi^e}{\partial y}\frac{\partial S_j}{\partial x}-\frac{\partial\psi^e}{\partial x}\frac{\partial S_j}{\partial y}\right)+\nu_o\left(\frac{\partial S_i}{\partial x}\frac{\partial S_j}{\partial x}+\frac{\partial S_i}{\partial y}\frac{\partial S_j}{\partial y}\right)\right]d\Omega\omega_j\right\}=$$

$$=\sum_{j=1}^{NN}\left\{\frac{b}{\rho_o}\left(\int_\Omega S_i\frac{\partial S_j}{\partial x}d\Omega\right)g_yC_j\right\} \tag{88}$$

In sequence, inserting the approximations of vorticity and stream function in the weak form of the Poisson Equation (Equation 62), one obtains

$$\sum_{j=1}^{NN}\left\{\int_{\Omega}\left(\frac{\partial S_i}{\partial x}\frac{\partial S_j}{\partial x}+\frac{\partial S_i}{\partial y}\frac{\partial S_j}{\partial y}\right)d\Omega\psi_j-\int_{\Omega}(S_iS_j)d\Omega\omega_j\right\}=0 \tag{89}$$

Equation 89 is hyperbolic and may be described in matrix form by:

$$[\mathrm{K}_0]\psi=[\mathrm{M}]\omega \tag{90}$$

Equations 85 and 88are parabolic and can also be put under matrix form as:

$$[\boldsymbol{M}]\left\{\dot{\omega}\right\}+([\mathrm{B}_1(\psi)]-[\mathrm{B}_2(\psi)]+\nu_o[\mathrm{K}_0])\{\omega\}=\{\boldsymbol{F}\} \tag{91}$$

where, $\left\{\dot{\omega}\right\}$ is the vorticity time derivative vector, [***M***] and {***F***} are either defined for outlet EBC or NBC, respectively, as:

$$[\mathrm{M}]=\sum_{j=1}^{NN}\left\{\int_{\Omega}S_iS_jd\Omega\right\} \tag{92}$$

and $$\{\mathrm{F}_o\}=\sum_{j=1}^{NN}\left\{\frac{b}{\rho_o}\left(\int_{\Omega}S_i\frac{\partial S_j}{\partial x}d\Omega\right)g_yC_j\right\} \tag{93}$$

or, for outlet MDBC, as:

$$[\mathrm{M}_2]=\sum_{j=1}^{NN}\left\{\left(\int_{\Omega}S_iS_jd\Omega+\frac{\nu_o}{\overline{U}}\int_{\Gamma_{out}}S_iS_jd\Gamma_{out}\right)\right. \tag{94}$$

and $$\{\mathrm{F}_1\}=\sum_{j=1}^{NN}\left\{\frac{b}{\rho_o}\left(\int_{\Omega}S_i\frac{\partial S_j}{\partial x}d\Omega+\frac{\nu_o}{\overline{U}}\int_{\Gamma_{out}}S_i\frac{\partial S_j}{\partial x}d\Gamma_{out}\right)g_yC_j\right\} \tag{95}$$

and last the matrices $[\mathrm{B}_1(\psi)]$ and $[\mathrm{B}_2(\psi)]$ are defined, respectively as:

$$\frac{\partial\psi^e}{\partial y}\frac{\partial S_j}{\partial x} \qquad \text{and} \qquad \frac{\partial\psi^e}{\partial x}\frac{\partial S_j}{\partial y} \tag{96}$$

In order to solve these equations, a time discretization formulation is adopted (SERT, 2015):

$$\{\omega_{t+1}\}=([\boldsymbol{M}]+\gamma\Delta t[\mathrm{KB}])^{-1}\left[([\boldsymbol{M}]-\Delta t(1-\gamma)[\mathrm{KB}])\omega_t+\Delta t((1-\gamma)\{\boldsymbol{F}\}_t+\gamma\{\boldsymbol{F}\}_{t+1})\right] \tag{97}$$

where:

$$[\mathrm{KB}]=[\mathrm{B}_1(\psi)]-[\mathrm{B}_2(\psi)]+\nu_o[\mathrm{K}_0] \tag{98}$$

which may be used for explicit and implicit solution schemes, depending on the value assigned to γ. If γ is set to zero, the scheme is an explicit forward differencing and if equal to 0.5 or 1, the scheme is implicit.

2.3.2 Computational code scheme

Taking advantage of the functions in MATLAB already developed for the species transport simulation, the code is now expanded to include stream function and vorticity simulations. Thus, all the previous features for evaluating integrals through GQ and the use of master elements in constructing the computational mesh are employed.

In view of the simple Galerkin formulation to be used, an implicit scheme for use in Equation 96, adopting $0.5 \leq \gamma \leq 1$, is naturally the preferred one. Although being computationally more demanding, it is known to be more stable compared to explicit schemes (SERT, 2015). Also, it is expected to control instabilities that may appear due to convection term of the governing equation.

For simplicity, in a scenario of limited computational resources, no other features for obtaining stable FEM simulations than mesh refining is employed. Thus, the use of schemes that do not have critical time steps restrictions seemed to be the best alternative.

The model is designed similarly to a cavity flow with water inflow from the left (west), outflow to the right (east). It was chosen this way due to the shape of reservoirs basins, mainly when a 2-D slice is taken to be studied. Also, its flow dynamics with recirculation and external induced flow patterns under the action of environmental effects are prone to be well represented in such scheme. Being a schematic case, no further considerations related to surface effects due to varying depth, like hydraulic jumps or surface level differences, are made.

A function was written for the code that automatically generates the mesh for the domain discretization (function gera_malha, see Appendix B), depicting an hypothetical basin and moving water surface. The shape profile is the one represented in Figure 14, supposed to depict an hypothetical reservoir basin with a dam wall. Meshes can be discretized as regular triangular and quadrangular and the numbers of GQ points for the calculation may be set from 3 to 9, according to the element shape.

Parameters of each individual flow run, namely, Reynolds and Froude numbers, are calculated with base on arbitrarily set fluid properties, as well as entrance depth and mean velocity.

2.3.3 Sketch of the algorithm

The algorithm developed to solve the feature system, comprising Equations 84 and 90, following uncoupling techniques mentioned by the studies cited before, is:

1) Initial conditions for vorticity, concentration and BCs for the stream function and concentration are prescribed;
2) Compute ψ_t from Equation 90;
3) Update ω_t from above computation of ψ_t;
4) Compute $\{F\}_{t+1}$ (Equations 93 or 95);
5) Compute ω_{t+1} from Equation 97;
6) To march in time, go back to step 2.

Step 3, above, is the adopted procedure for obtaining vorticity values at no-slip boundaries (Γ_2 and Γ_3) which are used as prescribed BC values for the vorticity field

computation. A relaxation procedure is employed in a reversal form of Equation 90 for the update of ω_t, or:

$$\omega_t = \alpha[\mathrm{M_o}]^{-1}[\mathrm{K_o}]\psi_t + (1-\alpha)\omega_t \tag{99}$$

where α is a relaxation parameter.

2.4 Preliminary Tests and Analysis

It is clearly shown by Equation 82, and other equations that follow, that stream function and vorticity computations and, in consequence, velocity profile simulations are dependent on the solute concentration profile as a source term that introduces the stratification of the flow. But, for these preliminary tests, this term was set to zero, because the concentration profile is not yet coupled.

Velocities profiles were calculated through the definition of a stream function for an incompressible flow, which implies in:

$$u_x = \frac{\partial \psi}{\partial y} \qquad \text{and} \qquad u_y = -\frac{\partial \psi}{\partial y} \tag{100}$$

The respective weak forms of the above equations are:

$$\int_\Omega w u_x d\Omega = \int_\Omega w \frac{\partial \psi}{\partial y} d\Omega \qquad \text{and} \qquad \int_\Omega w u_y d\Omega = -\int_\Omega w \frac{\partial \psi}{\partial x} d\Omega \tag{101}$$

Now, by applying GFEM and taking Equation 84 into account one obtains:

$$\sum_{j=1}^{NN}\left(\int_\Omega S_i S_j d\Omega\right)\mathrm{u}_j = \sum_{j=1}^{NN}\left(\int_\Omega S_i \frac{\partial S_j}{\partial y} d\Omega\right)\psi_j \tag{102}$$

and:

$$\sum_{j=1}^{NN}\left(\int_\Omega S_i S_j d\Omega\right)\mathrm{v}_j = -\sum_{j=1}^{NN}\left(\int_\Omega S_i \frac{\partial S_j}{\partial x} d\Omega\right)\psi_j \tag{103}$$

which can be respectively put in matrix form for computation as:

$$[\mathrm{M_o}]\mathrm{u} = [G]\psi \qquad \text{and} \qquad [\mathrm{M_o}]\mathrm{v} = [H]\psi \tag{104}$$

where $[H]$ and $[G]$ are, respectively:

$$\sum_{j=1}^{NN}\left(\int_\Omega S_i \frac{\partial S_j}{\partial y} d\Omega\right)\psi_j \text{ and} \qquad -\sum_{j=1}^{NN}\left(\int_\Omega S_i \frac{\partial S_j}{\partial x} d\Omega\right)\psi_j \tag{105}$$

Figure 15 – Stream function computations for Re = 100

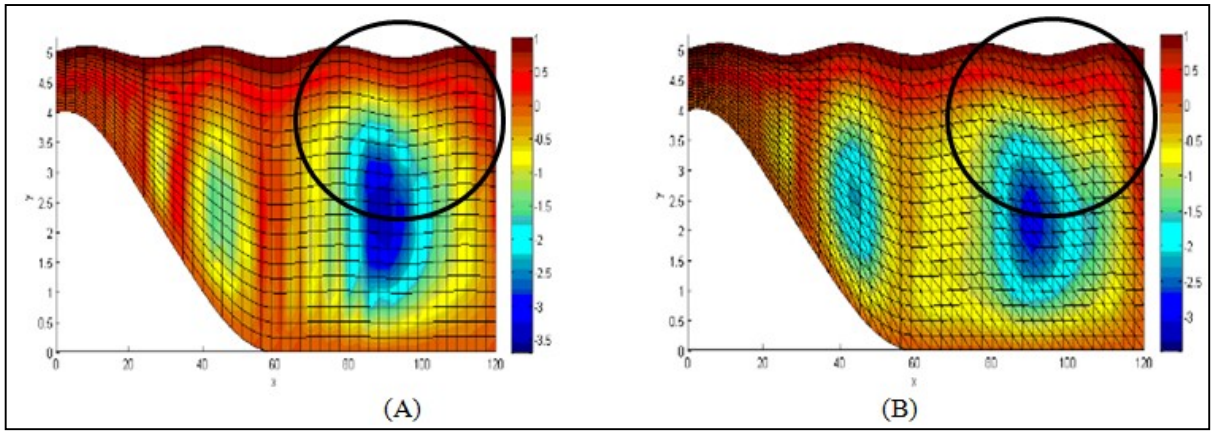

Tags: (A) – Oulet NBC; (B) – Outlet EBC.

In the first tests performed, computations of stream function that took NBC as the outlet BC in Equation 62 showed oscillations which rarely happened when the BC was imposed (highlighted in Figure15). It was observed that these oscillations were often followed by instabilities after some computation time. A comparative plot in one dimension along the flow quantifies these oscillations (Figure 16) and indicates that they are smoothed if EBC is used, even when the outlet BC for vorticity transport is NBC or MDBC.

Figure 16 – Stream function 1-D plots at arbitrary depth of 2.5 for Re=100

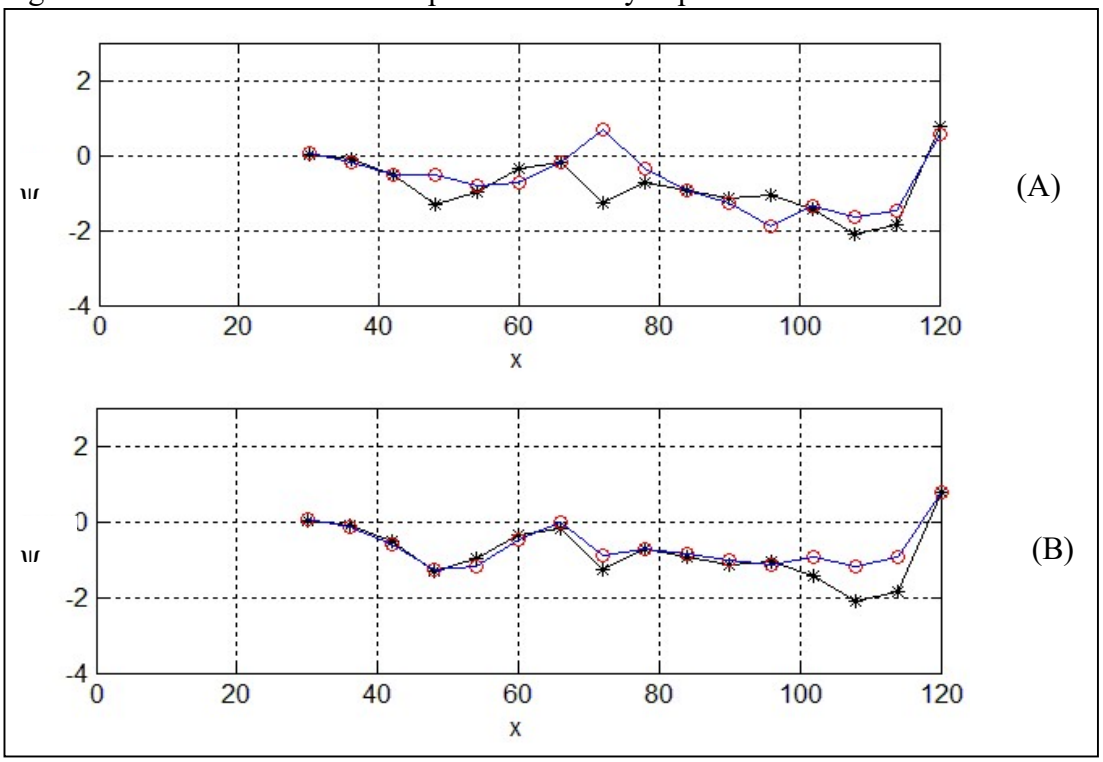

(A)– outlet EBC for stream function and vorticity computation: —*—
outlet NBC for stream function and vorticity computation: ○
outlet NBC for stream function and MDBC for vorticity computation : ——

(B) – outlet EBC for stream function and vorticity computation: —*—
outlet EBC for stream function and NBC for vorticity computation: ○
outlet EBC for stream function and MDBC for vorticity computation : ——

Under the proposed conditions, the stream function must assume values from zero to one at the outlet surface that are, in practical terms, imposed. So, the use of outlet NBC for its computation may be an inconsistency that could contribute to some of the observed instabilities. It was then decided to run stream function computations with outlet EBCs only, letting NBC and MDBC exclusively as outlet conditions for vorticity and velocity computations.

Some of the instabilities found were also due to poor conditioning of the constructed matrices. Use of preconditioners, as well as of more elaborated finite element schemes were not in consideration in this thesis, but proper mesh refining contributed to extend significantly the possibilities of the simulation. After some polishing of the source code, simulation up to 2000 elements mesh were run under acceptable computational times, even with the limited hardware at hand.

Selected outcomes are shown for the same arbitrary time lapse and moderate Reynolds Numbers which are evaluated by assuming the unitary depth entrance as the characteristic length.

It is clear that the numerical scheme can capture stream function and vorticity transport and by consequence, flow velocity profiles. Simulations run for 1800 elements mesh of regular triangular shape are following shown.

It is to note that some of these preliminary tests were run trying to represent cyclic moving surfaces, in order to simulate waves and the characteristic reservoirs' seiches that imply in surface level differences (PACHECO, 2009). Figures 15, 20 and those of Appendix A illustrate this attempt that is programmed in function gera_malha (Appendix B). However, due to time and hardware limitations this feature was not further explored.

2.4.1 Velocity profiles with no wind on the reservoir surface

Longitudinal velocity profiles in the case of zero surface vorticity (ω_s), that correspond to no tangential blowing wind on the reservoir surface, are depicted in Figures 17 to 19. Varied outlet BCs were tested in order to check the code. Vorticity and Stream Function plots are also shown in order to verify the pattern change due to the Reynolds Number. Vertical velocities profiles were also captured, denoting the 2-D flow character (Figure 20). A more comprehensive set of results is shown in Appendix A.

Figure 17 – Stream function, vorticity and longitudinal velocity computation (Re = 100; ω_s =0.0; outlet EBC; GQ of seven points).

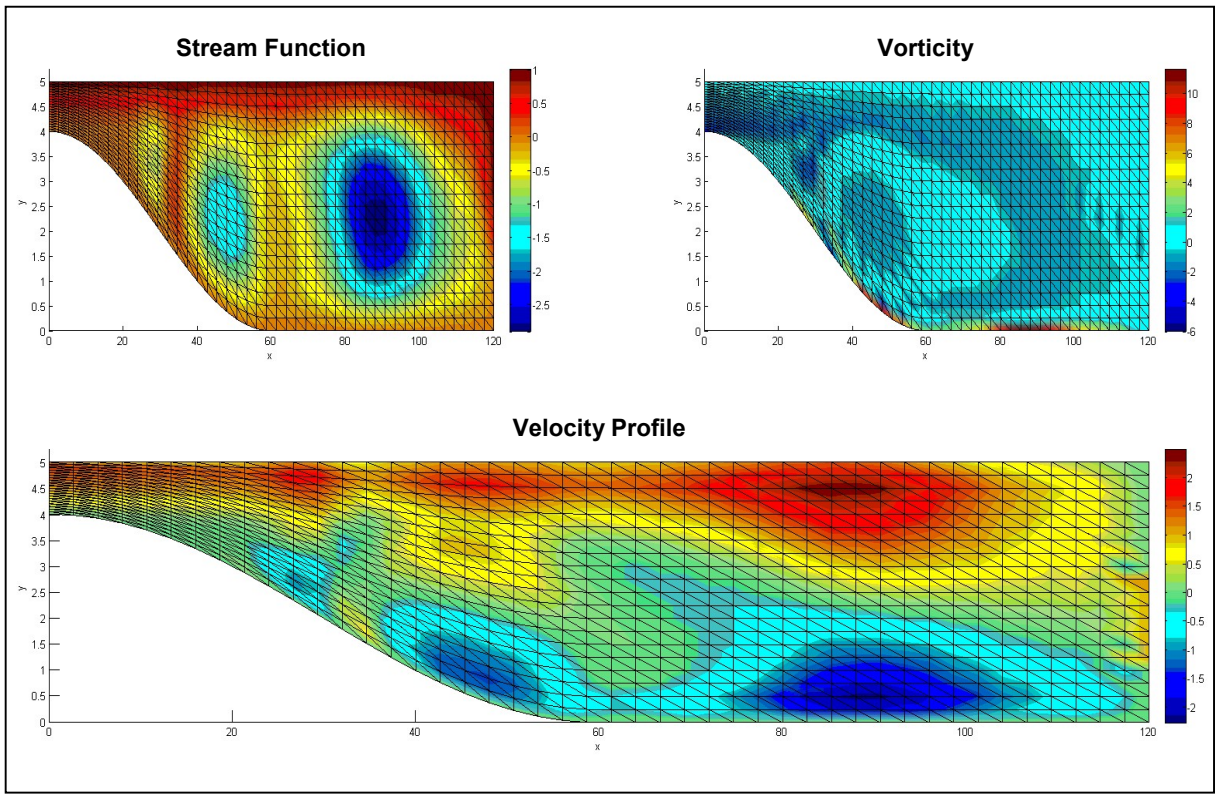

Figure 18 – Stream function, vorticity and longitudinal velocity computation (Re = 500; ω_s =0.0; outlet NBC; GQ of seven points).

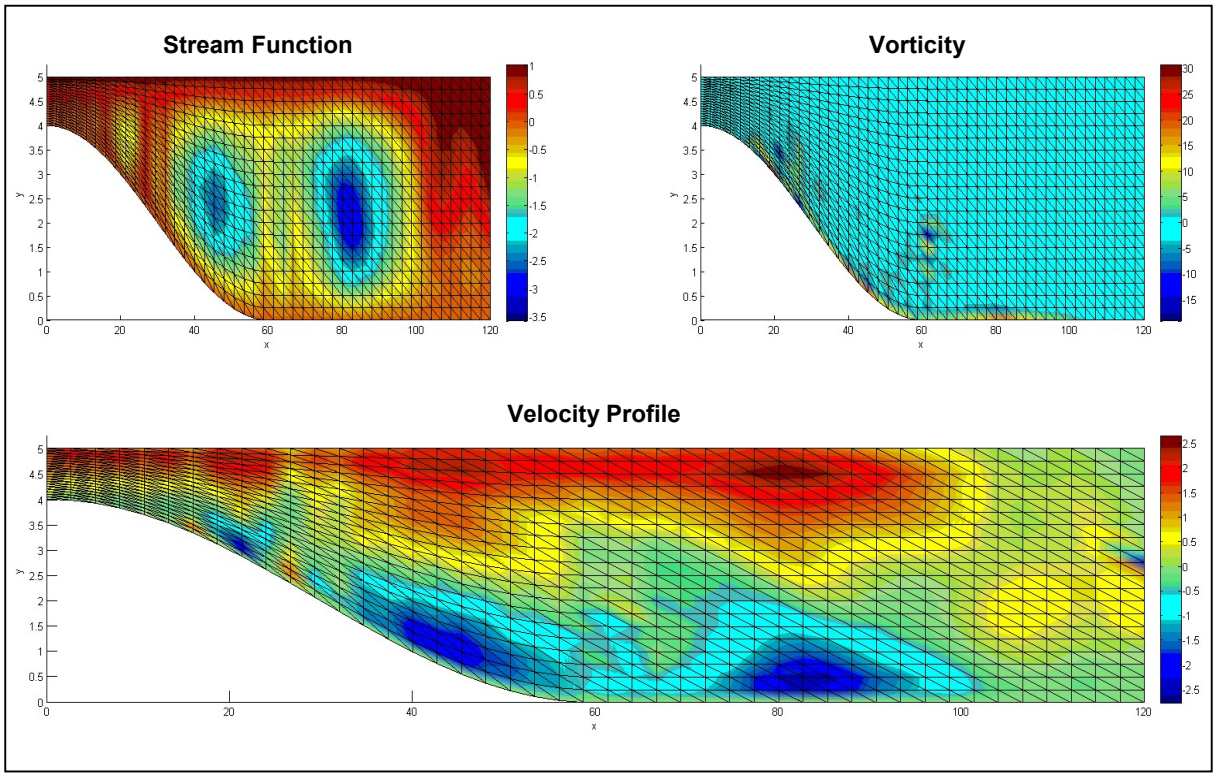

Figure 19 – Stream function, vorticity and longitudinal velocity computation (Re = 1000*;* ω_s =0.0; outlet MDBC; GQ of seven points).

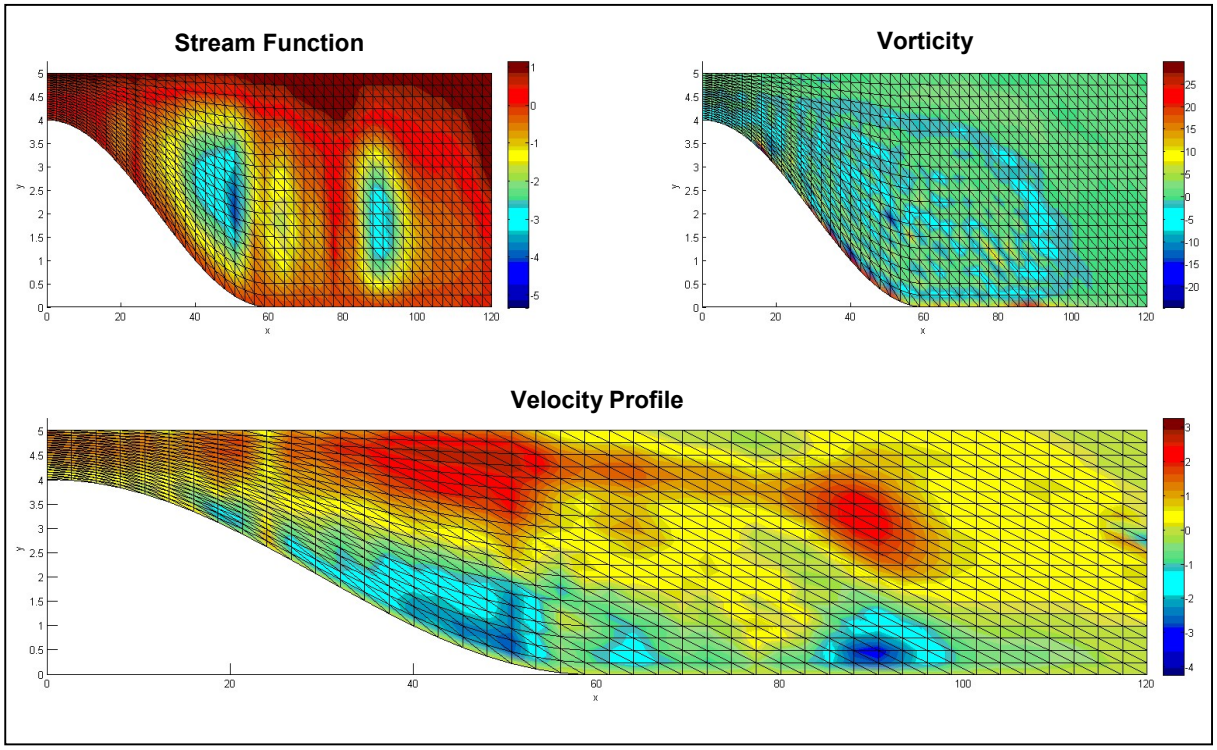

Figure 20 – Vertical velocity computations for selected Re and outlet BCs (ω_s =0.0; GQ of seven points).

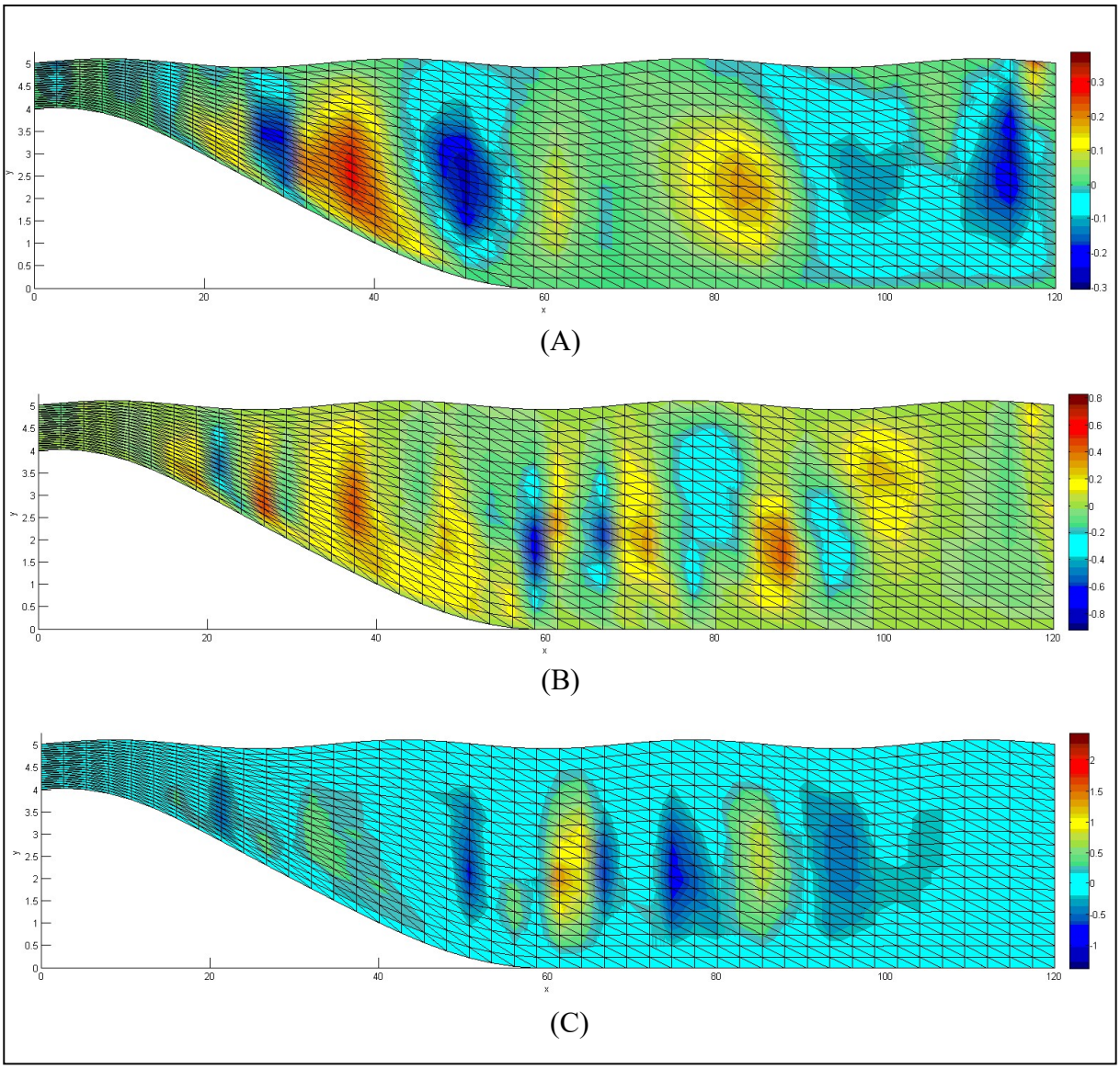

Tags: (A) – Re = 100; outlet EBC; (B) – Re = 500; outlet NBC; (C) – Re = 1000; outlet MDBC.

2.4.2 Velocity profiles with wind blowing on the reservoir surface

In order to demonstrate effects of blowing wind on the surface, tangential surface vorticity is arbitrarily set to 1.0 and -1.0, what simulates surface stresses induced, respectively, by wind blowing against and in favour of the flow longitudinal direction. These winds modify the entrance velocity and stress profiles (see Equations 75 to 78), implying in modification of flow parameters and of the calculated profiles, as shown by Figures 21 and 22.

It can be seen that simulations respond accordingly. When a contrary wind is prescribed, the velocity profile is retarded and the flow is plunged towards the bottom. On the contrary, when the wind is favourable to the flow, velocities are accelerated at the surface and greater difference of velocities from reservoir surface to the bottom are observed.

As to remark differences in computation of stream function and vorticity for the simulation of surface wind blowing, these functions are again plotted and shown.

Figure 21 – Stream function, vorticity and longitudinal velocity computation (Re = 500; ω_s =1.0; outlet MDBC; GQ of seven points).

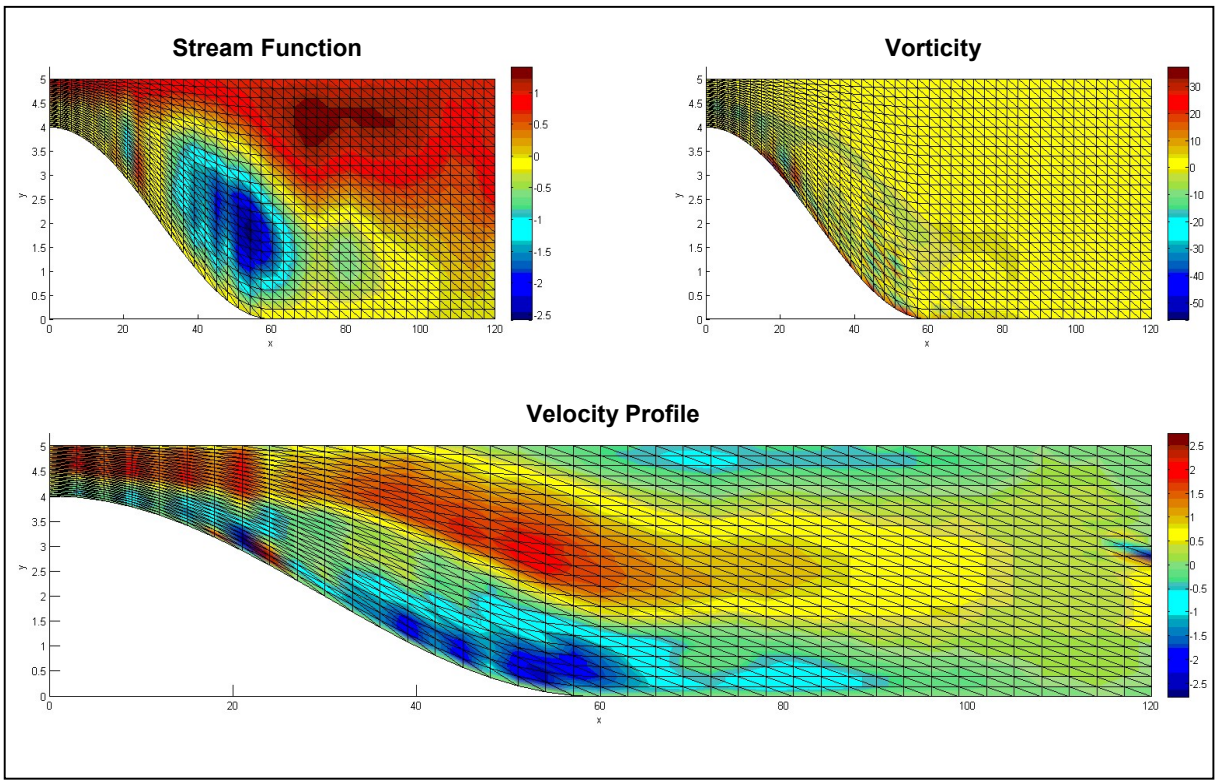

Figure 22 – Stream function, vorticity and longitudinal velocity computation (Re =100; ω_s = -1.0; outlet NBC; GQ of seven points).

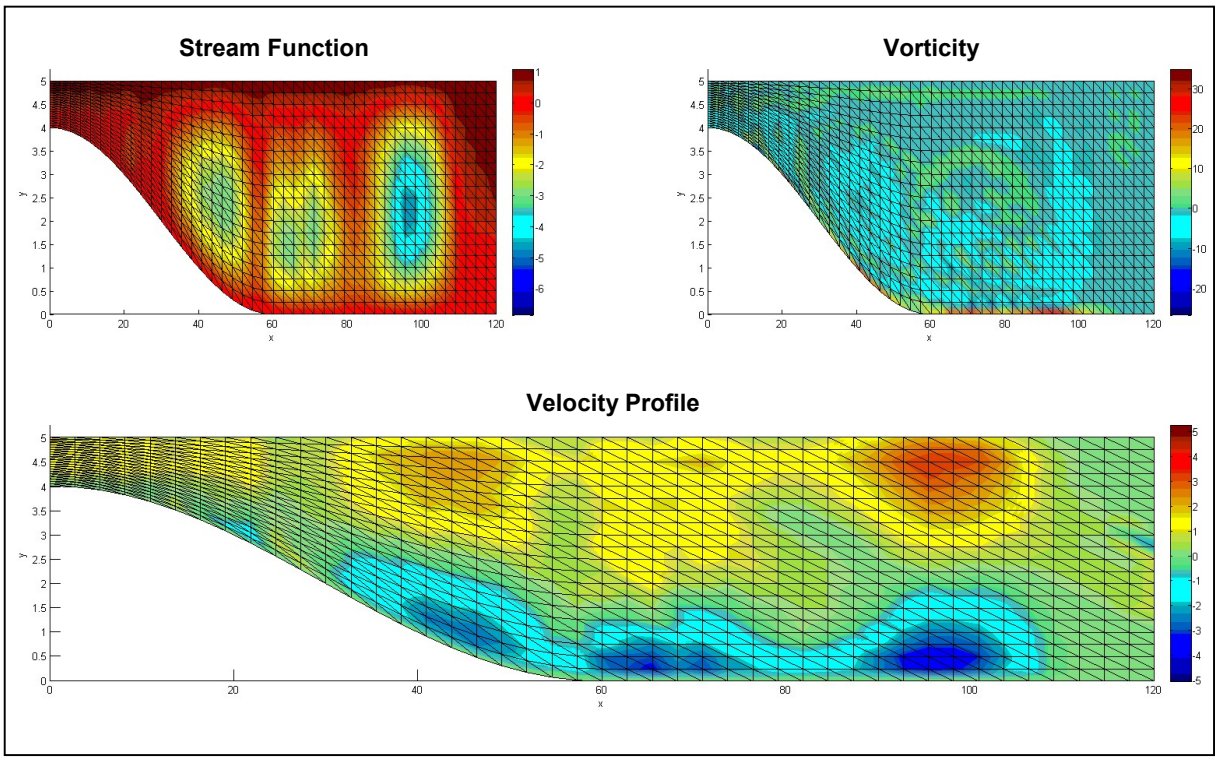

2.4.3 Cyclic environmental effects simulation

It is understood that environmental induced variations of flow conditions should also be prone to be simulated by the code. So, as stated earlier, periodic inlet flow velocities would imply in periodic stream function and vorticity, which also implies in periodic changing boundary values in all surfaces. This is a very particular case of problem which is also explored and following shown (Figure 23).

Figure 23 – Stream function, vorticity and longitudinal velocity computation (Re = 100; ω_s =0.0; outlet MDBC; GQ of seven points).

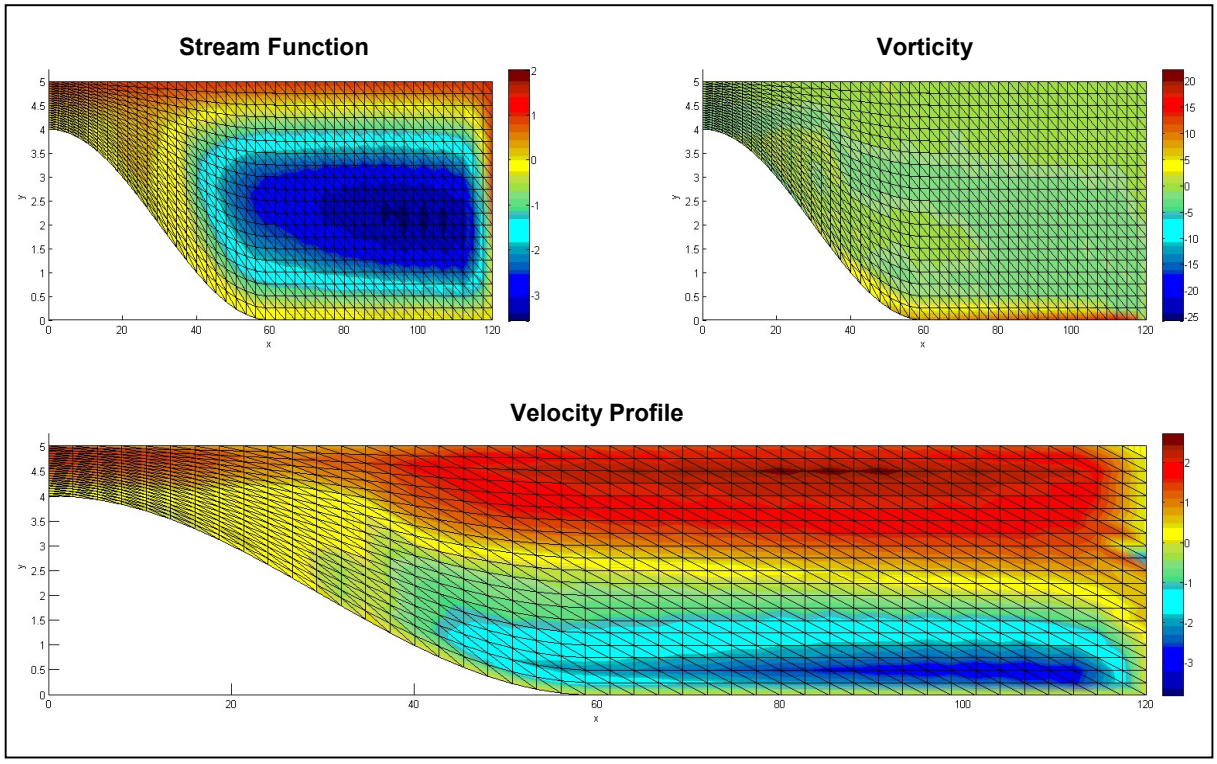

A more consistent problem of cyclic environmental variation may is matched by considering that only the surface condition is affected by an external wind whose magnitude periodically varies. This implies in keeping all the other BCs, resulting in a better posed problem, which examples are shown in Figures 24 and 25.

Figure 24 – Stream function, vorticity and longitudinal velocity computation (Re =100; ω_s = 1+$cos2\pi t$; outlet MDBC; GQ of seven points).

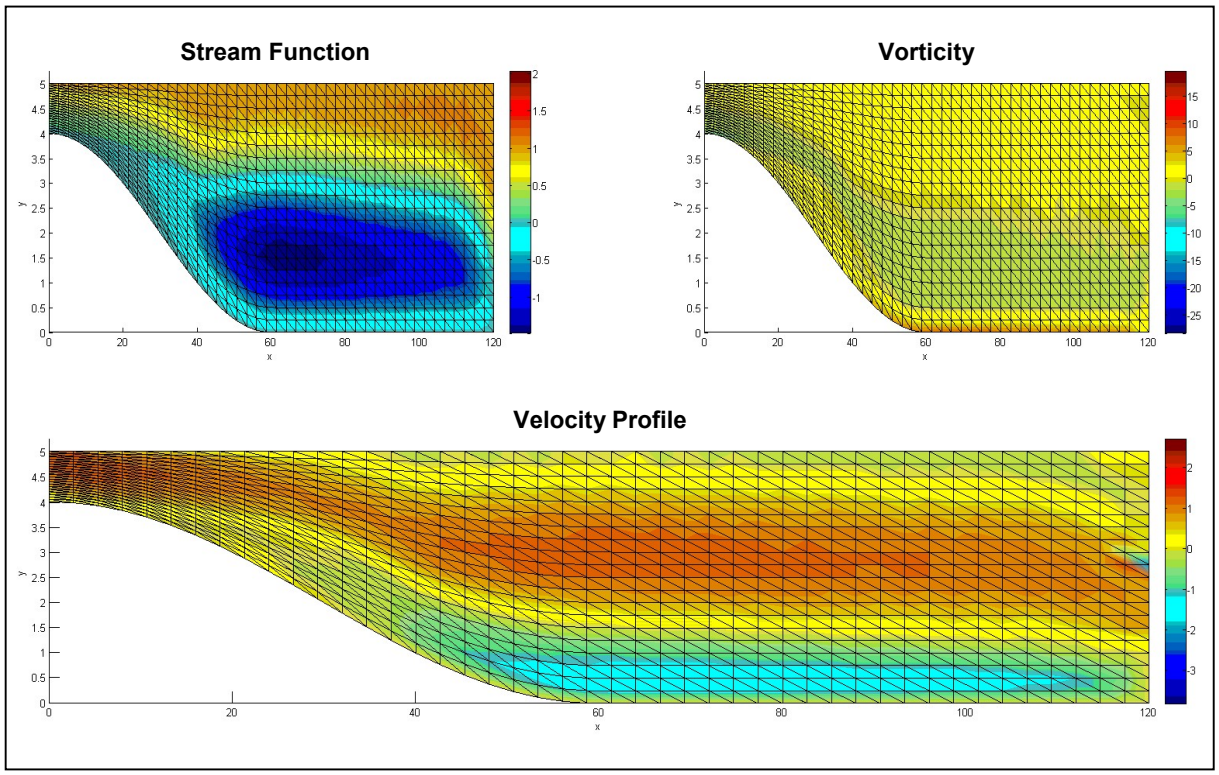

Figure 25 – Stream function, vorticity and longitudinal velocity computation (Re =100; ω_s = – (1+$cos2\pi t$); outlet MDBC; GQ of seven points).

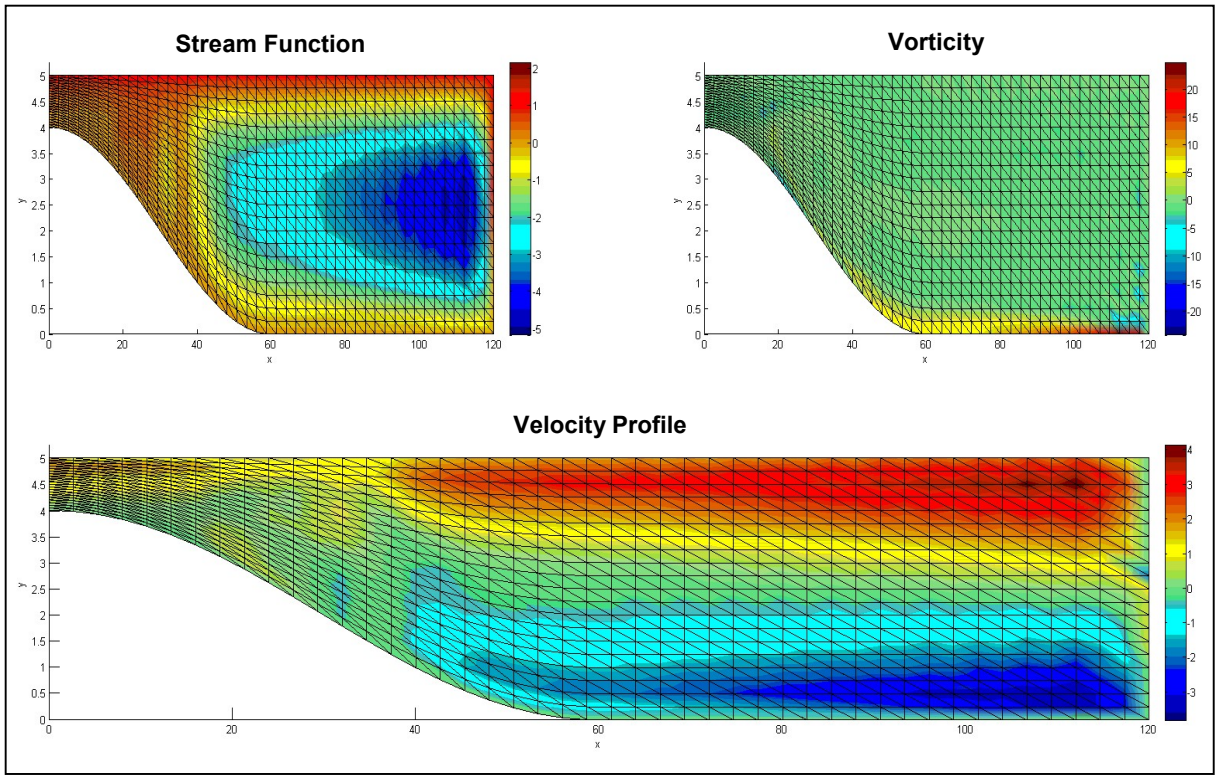

An outcome is also shown below (Figure 26), for a flow starting with no wind blowing ($\omega_s = 0$) which, after an arbitrary time, is affected by an opposite wind ($\omega_s = 1$) and, later, by a wind in the same direction of the flow ($\omega_s = -1$).

Figure 26 – Stream function, vorticity and longitudinal velocity computation (Re =100; alternate surface vorticity; outlet MDBC; GQ of seven points).

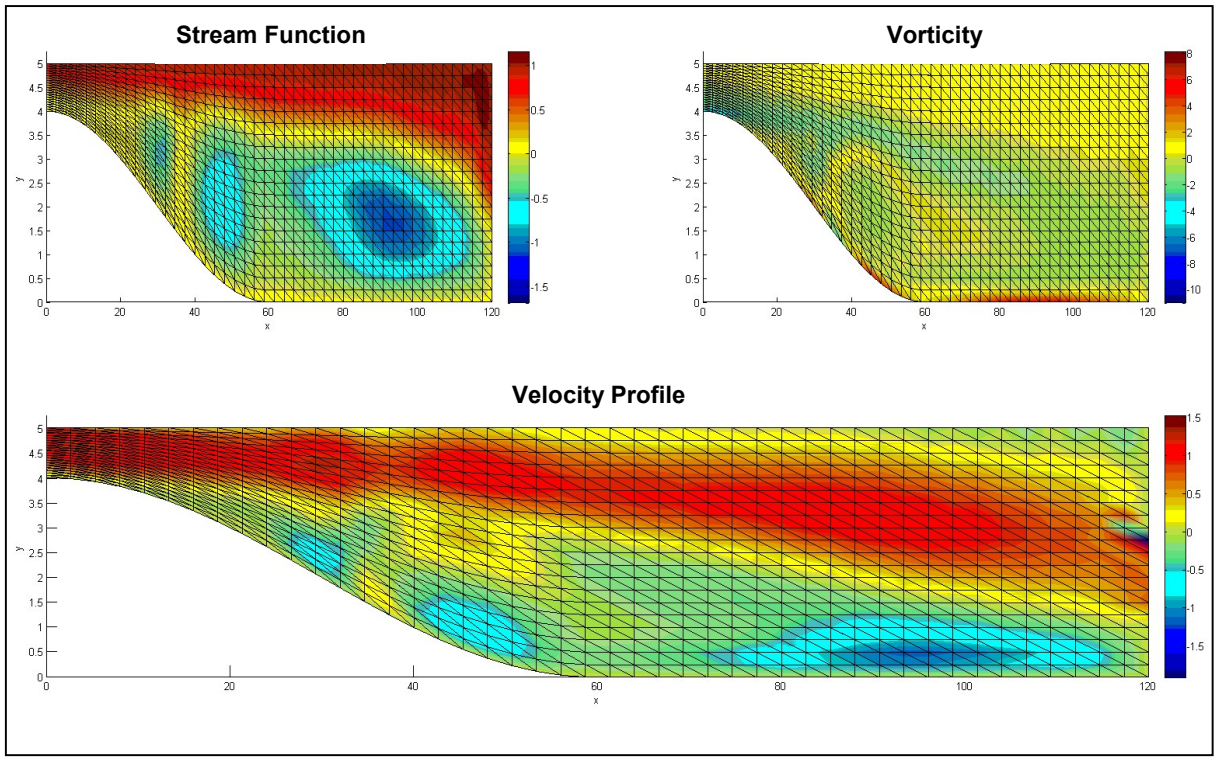

The outcomes of Figures 21 to 26 indicate different flow patterns due to cyclic variations. However, it may be observed that the typical cycle of such variations does not happen in the same adopted time scale, which was used only in order to make feasible the analysis within a reasonable observation time.

It is hard to figure out in a static figure all the dynamic of such variations but it may be observed that the simulated velocity profile pattern, and also the ones of stream function and vorticity, are different for the same Reynolds Number computed.

2.4.4 Velocity profiles simulation with buoyant term

In order to take the buoyant term in consideration, it is obviously necessary to compute the gas concentration of the domain. Equation 23, however, requires the velocity profile, that is not yet defined. Thus, coupling of the velocity profile may be attained by introducing the stream function in that equation, resulting in:

$$\sum_{j=1}^{NN}\left\{\left(\int_{\Omega} S_i S_j d\Omega + \frac{D_x}{\overline{U}}\int_{\Gamma_{out}} S_i S_j d\Gamma_{out}\right)\frac{dC_j}{dt} + \int_{\Omega}\left[S_i\left(\frac{\partial\psi^e}{\partial y}\frac{\partial S_j}{\partial x} - \frac{\partial\psi^e}{\partial x}\frac{\partial S_j}{\partial y}\right) + \left(D_x\frac{\partial S_i}{\partial x}\frac{\partial S_j}{\partial x} + D_y\frac{\partial S_i}{\partial y}\frac{\partial S_j}{\partial y}\right)\right]d\Omega C_j - k\left(\int_{\Omega} S_i S_j d\Omega + \frac{D_x}{\overline{U}}\int_{\Gamma_{out}} S_i S_j d\Gamma_{out}\right)C_j\right\} = 0 \qquad (106)$$

Once the concentration profile is computed, it is introduced in Equations 85 or 88, depending on the case run. Velocities, now for a fully stratified domain, resulting from incorporating density variation due to gas concentration may be reached. A constant *b* parameter, arbitrarily chosen, by its turn, imposes initially a linear gas concentration profile as depicted in Figure 5. Equation 106 corresponds to the computation with MDBC at the outlet. If imposed or natural BCs are used, this equation, without the surface integrals also applies.

For the outcomes shown, concentration profiles are obtained subjected to imposed BC at the inlet and at the bottom of the reservoir and NBC or MDBC at the surface and exit. With reference in the scheme of Figure 14, this is:

a) on Γ_{in}: $C_{in} = 0.0$; (107)

b) on Γ_1: $C_1 = 0.0$ or $C_1 = (1 + cos\ m\pi t)$ for the gas evolution spots; (108)

c) on Γ_2 and Γ_{out}: $\dfrac{\partial C}{\partial x} = 0$, or: $\left(\dfrac{\partial C}{\partial t} + \overline{u}_x \cdot \dfrac{\partial C}{\partial x}\right)\Big|_{\Gamma_i} = -kC|_{\Gamma_i}$ (109)

Figure 27 – Stream function, vorticity and longitudinal velocity computation (Re = 100; ω_s = 0.0; outlet NBC).

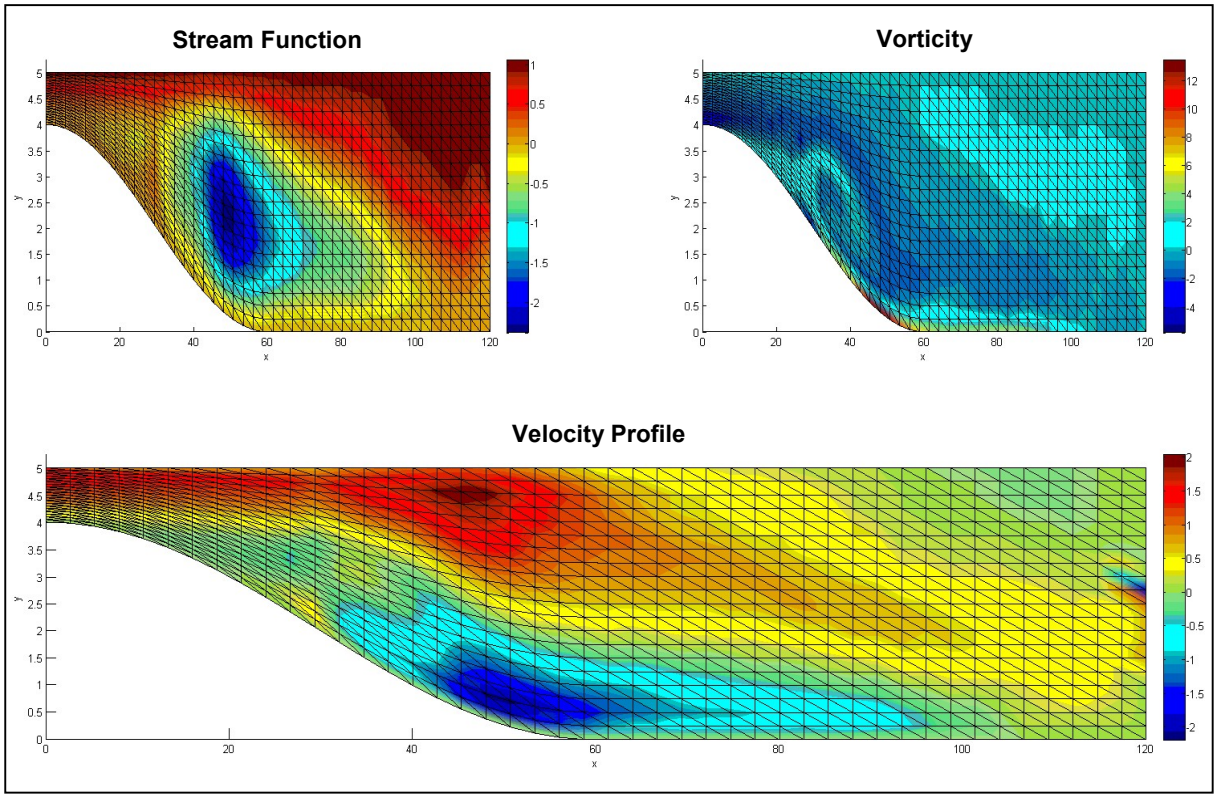

Figure 28 – Stream function, vorticity and longitudinal velocity computation (Re = 100; ω_s = 1.0; outlet MDBC).

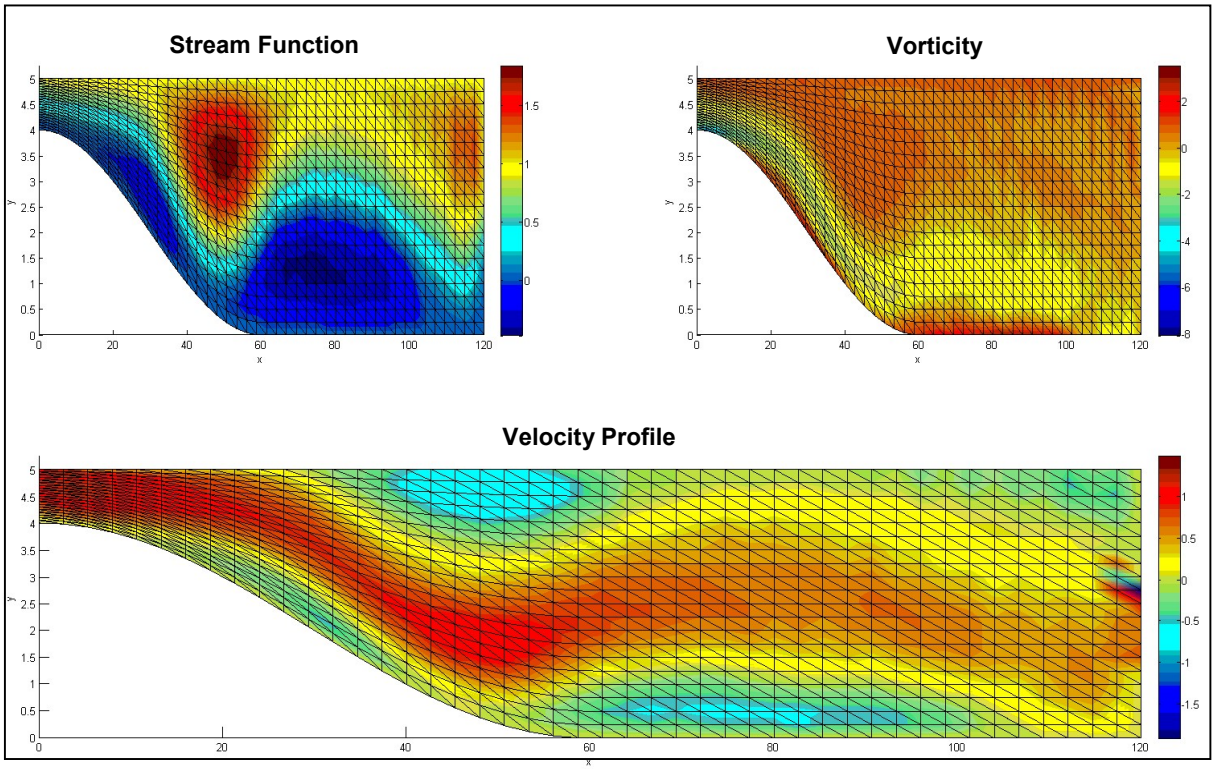

Figure 29 – Stream function, vorticity and longitudinal velocity computation (Re = 100; ω_s = - 1.0; outlet MDBC).

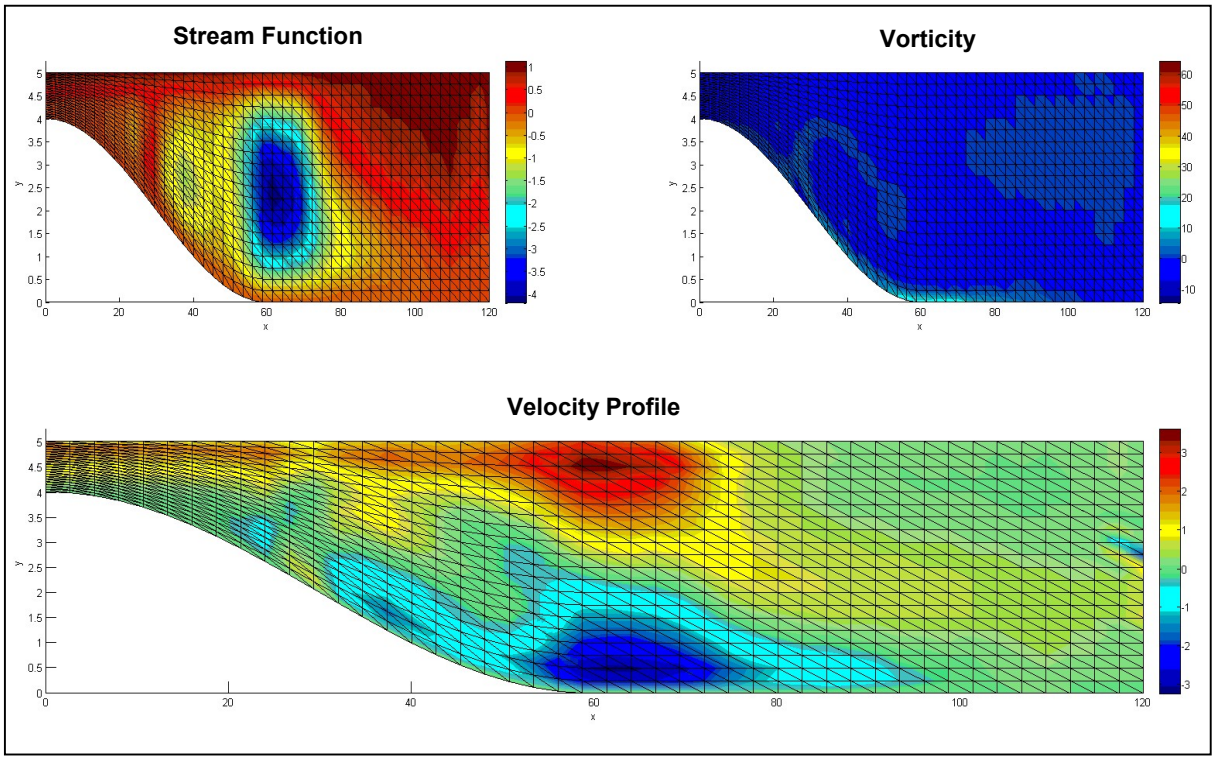

Situations simulated also included cases of wind blowing at the water surface (Figures 28 and 29). If above figures are compared to others related to the same Re, it is noted that stream-function and vorticity profiles develop differently when mass is added. As consequence, velocity profiles also develop differently, all affected by fluid density variations due to gas concentration distribution within the domain. It is also interesting to note that wind blowing, modifying fluid stress distribution, also contributes to fluid stratification.

2.5 **Model Verification**

The results of the tests allow the conclusion that the model was built in the correct way, meaning that the conceptual model is correctly represented by the computer code that implements that conception. However, it was still necessary to provide its verification, in order to check the outcomes.

Nevertheless, results fitting to the cases studied and that could be used as benchmarks have not been found in the literature. On the other hand, lid-driven cavity flow problems results are widely published. Thus, it was decided to approach verification by applying the code to lid-driven cavity flow problems.

BCs were then modified and routines related to concentration and velocity profiles were deactivated but the core of the algorithm was kept untouched. Tests were run for Reynolds Numbers of 100, 400 and 1000, which cover the span of simulations intended for the problem under investigation. The result for Re = 100 was obtained through the use of a 1800 triangular mesh, for Re = 400, 1600 quadrangular mesh and for Re = 1000, 2025 quadrangular mesh. The same arbitrary nondimensional time of 10.0, when steady conditions were approached, with time step of 0.01 was used.

Figure 30 illustrates the outcomes and Table 6 compares selected data for extremum stream function values and corresponding vorticity. It is verified that most results agree with those of cited literature.

Figure 30 – Lid-driven cavity stream function computations for selected Reynolds numbers.

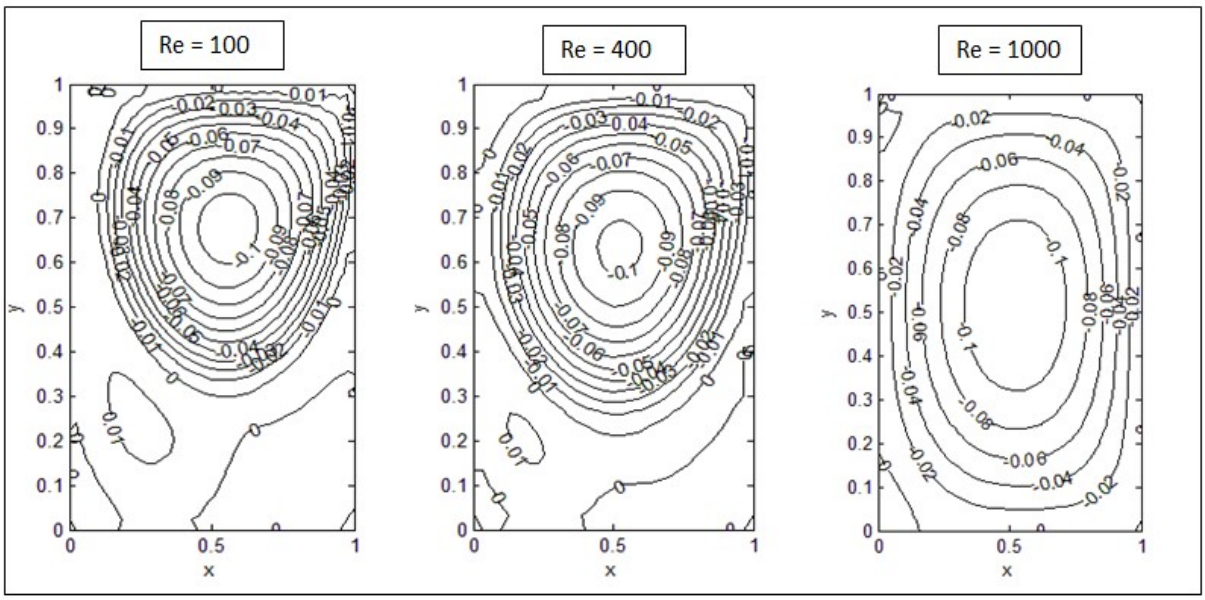

Table 6 – Comparison of literature and obtained stream function and vorticity

Re	Primary vortex location				Stream function/vorticity			
	Literature		Simulation		Literature		Simulation	
	x	y	x	y	ψ	ω	ψ	ω
100	0.62(a; b)	0.73(a; b)	0.55	0.68	-0.103(a; b)	3.167(a)	-0.103	2.801
400	0.56(a; b)	0.61(a; b)	0.53	0.63	-0.114(a; b)	2.295(a)	-0.106	2.833
1000	0.53(b; c)	0.57(b; c)	0.53	0.51	-0.119(b; c)	2.065(c)	-0.120	2.197

Source: (a) – Ghia et al. (1982); (b) –Marchi et al. (2009); (c) – Erturk et al (2005).

The code was also verified by comparing its outcomes to published data for velocity profiles in the two directions at cavity center (MARCHI et al., 2009), covering the span of Reynolds Numbers that apply to the problem under study (Figures 31 and 32).

Figure 31 – Lid-driven cavity u at $x = 0.5$ and v at $y = 0.5$ for Re = 10 and Re = 100

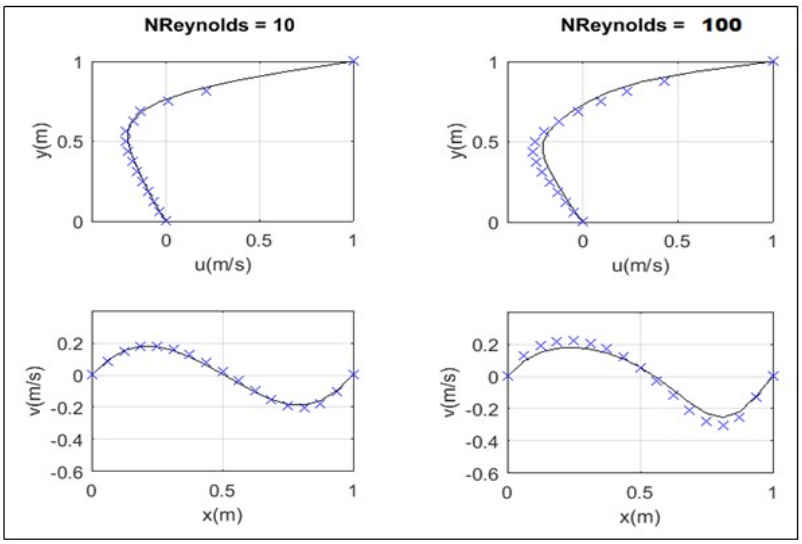

Tags: ——— (MARCHI et al., 2009); xxx (this thesis).

Figure 32 – Lid-driven cavity u at x = 0.5 and v at y = 0.5 for Re = 400 and Re = 1000

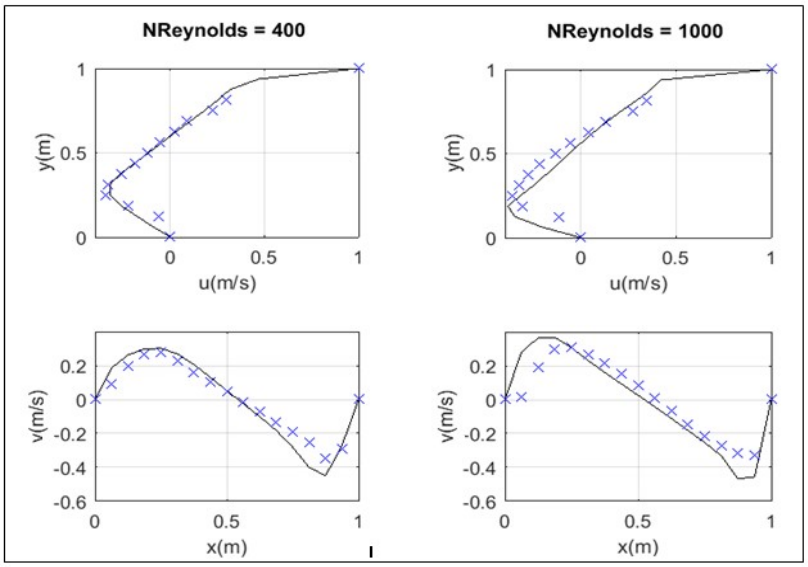

Tags: ——— (MARCHI et al., 2009); xxx (this thesis).

From the analysis of the above figures, again it may be verified that results mostly agree with benchmark data. Slight discrepancies observed may be credited to differences in mesh refining and program resources. For instance, the results of Marchi et al. (2009) were obtained with a 1024 x 1024 grid, while the ones of this thesis were obtained through a rough 21 x 21 mesh, which was, however, able to capture reliable results. It is also observed a tendency to derive from benchmark data as the Reynolds Number increases.

It must be remarked that the analysis was difficult to carry on, also because published data are sometimes not very clearly presented and often diverge for supposedly similar conditions. Comini et al (1994), Wright & Gaskel (1995) and Erturk (2005), for instance, study some discrepancies that may appear due to different grids, methods and time steps. Besides, in this thesis, the finite element formulation relies simply on Galerkin method for space discretization without any upwinding technique, mostly used in benchmark works, that may imply deviations of the results. Yet, it was possible to reach more or less stable solutions up to Re=1000 by properly refining the mesh and adopting the fully implicit method for time discretization.

Finally, having these in mind , it may be concluded that the test results indicate that the code reproduces favourably lid-driven cavity flow benchmark data.

2.6 **Closure**

The computation of reactive flows velocity profiles that occur in hydroeletric reservoirs where gases evolve from the bottom and react in their path to the surface is presented. This profile applies to a stratified flow case due to density variation caused by the presence of gases in the water and also to external changing environmental conditions. The aim is to couple the velocity profile to the species concentration in a nonlinear system that could be used to simulate the concentration profile in such basins.

The flow was modeled in a novel way, by using vorticity-stream function formulation where density changes are incorporated in a buoyant term, itself coupled to the gas concentration profile, introduced by the Boussinesq hypothesis. The MDBC concept, developed in Section 1, was applied and velocity profiles were obtained for a range of chosen situations.

In the absence of a specific benchmark for the problem, the code was tested by applying it to the classical lid-driven cavity flow, allowing its verification. It was found that the use of a simple GFEM scheme and coarse meshes implies in better performance for lower Reynolds Numbers, what seems to restrict its use to moderate flow velocities, but it is within the range of reservoir flow regimes intended for the investigation.

Thus, it is now possible to pursue the simulation of reactive gases concentration for this environment, what is done in the next section.